Atmos. Meas. Tech. Discuss., 7, 5559–5599, 2014
www.atmos-meas-tech-discuss.net/7/5559/2014/
doi:10.5194/amtd-7-5559-2014

Atmospheric Measurement Techniques Discussions
Open Access

An improved glyoxal retrieval from OMI measurements

L. M. A. Alvarado[1], A. Richter[1], M. Vrekoussis[2], F. Wittrock[1], A. Hilboll[1], S. F. Schreier[1], and J. P. Burrows[1]

[1]Institute of Environmental Physics (IUP), University of Bremen, Bremen, Germany
[2]Energy, Environment and Water Research Center, The Cyprus Institute, Nicosia, Cyprus

Received: 17 April 2014 – Accepted: 26 May 2014 – Published: 5 June 2014

Correspondence to: L. M. A. Alvarado (lalvarado@iup.physik.uni-bremen.de)

Published by Copernicus Publications on behalf of the European Geosciences Union.

Abstract

Satellite observations from the SCIAMACHY, GOME-2, and OMI spectrometers have been used to retrieve atmospheric columns of glyoxal (CHOCHO) with the DOAS method. High CHOCHO levels are found over regions with large biogenic and pyrogenic emissions, and hot-spots have been identified over areas of anthropogenic activities.

This study focuses on the development of an improved retrieval for CHOCHO from measurements by the OMI instrument. From sensitivity tests, an optimal fitting window and polynomial degree are determined. Two different approaches to reduce the interference of liquid water absorption over oceanic regions are evaluated, achieving significant reduction of negative columns over clear water regions. Moreover, a high temperature absorption cross-section of nitrogen dioxide (NO_2) is introduced in the DOAS retrieval to account for potential interferences of NO_2 over regions with large anthropogenic emissions, leading to improved fit quality over these areas. A comparison with vertical CHOCHO columns retrieved from measurements of the GOME-2 and SCIAMACHY instruments over continental regions is performed, showing overall good consistency.

Using the new OMI CHOCHO data set, the link between fires and glyoxal columns is investigated for two selected regions in Africa. In addition, mapped averages are computed for a fire event in the east of Moscow between mid-July and mid-August 2010. In both cases, enhanced CHOCHO levels are found in close spatial and temporal proximity to MODIS fire radiative power, demonstrating that pyrogenic emissions can be clearly identified in the OMI CHOCHO product.

1 Introduction

Volatile organic compounds (VOC) are chemical species emitted from biogenic, pyrogenic, and anthropogenic sources. In spite of their small mixing ratios, usually a few

AMTD
7, 5559–5599, 2014

parts per trillion (pptv) to several parts per billion (ppbv), VOC significantly influence the ambient atmospheric composition with direct and indirect impacts on atmospheric chemistry and climate change (Williams, 2004; Curci et al., 2010; Vrekoussis et al., 2010). Enhanced levels of VOC in combination with nitrogen oxides ($NO_x = NO + NO_2$) lead to the photochemical formation of ozone (O_3) (e.g., Houweling et al., 1998). Additionally, VOC contribute to the formation of secondary organic aerosols (SOA) (Fu et al., 2008) and to cloud condensation nuclei (CCN) formation (e.g., Yu, 2000).

VOC include non-methane hydrocarbons (NMHC) and oxygenated NMHC (OVOC, e.g., alcohols, aldehydes, organic acids), emitted from various natural and anthropogenic sources such as vegetation, oceans, fossil fuel burning, biomass burning, as well as geochemical processes (Kansal, 2009). On a global scale, biogenic VOC sources (BVOC refers to VOC from biogenic sources) result in an annual release of 1150 Tg C yr^{-1} (Guenther et al., 1995), mainly emitted in the form of isoprenes (C_5H_8) and monoterpenes (varieties of molecules with two isoprene units) (Guenther et al., 1995; Atkinson and Arey, 2003; Kansal, 2009). However, the uncertainties in total emissions are high since the amounts emitted depend on several parameters, including the plant species, temperature, humidity, and also the condition of the plant (Guenther et al., 2000). In urban areas, VOC from anthropogenic emissions (AVOC) are emitted from mobile and stationary sources (Kansal, 2009). However, estimated AVOC emissions of 161 Tg C yr^{-1} are 10 times lower than the respective BVOC. Lastly, 49 Tg C yr^{-1} emanate from pyrogenic emissions (Andreae and Merlet, 2001). Similar to the biogenic emissions, the total amount of the pyrogenic emissions of VOC is largely uncertain (Stavrakou et al., 2009b). The inhomogeneous spatial and temporal distribution of the various VOC, resulting in a large variability of VOC fluxes into the atmosphere, led several research groups to study the global distribution of smaller molecules such as formaldehyde (HCHO) and CHOCHO, which are produced from precursor BVOC and AVOC species. Also pyrogenic emissions give directly and indirectly HCHO and CHOCHO. CHOCHO, the smallest of the alpha-dicarbonyls and one of the most prevalent carbonyls in the atmosphere (Myriokefalitakis et al., 2008), is often used as a tracer

AMTD
7, 5559–5599, 2014

of hydrocarbons over areas with enhanced VOC emissions, the so-called photochemical "hot-spot" regions. CHOCHO is an intermediate product in the oxidation of most VOC (Volkamer et al., 2005a; Wittrock, 2006; Sinreich et al., 2007) and an indicator of secondary organic aerosol formation (Sinreich et al., 2007; Fu et al., 2008; Vrekoussis et al., 2009). Glyoxal is mainly produced from the oxidation of isoprene, acetylene, and aromatic hydrocarbons (Fu et al., 2008; Liu et al., 2012) and has a short atmospheric lifetime on the order of a few hours (Atkinson, 2000), with photolysis being its dominant sink (Tadić et al., 2006). Other sinks comprise wet and dry deposition (Fu et al., 2008), SOA formation (Volkamer et al., 2007, and references therein), and the oxidation mechanism, which is driven by the presence of hydroxyl radicals (Setokuchi, 2011).

In recent years, measurements from space-born instruments, including the SCanning Imaging Absorption spectroMeter for Atmospheric CHartographY (SCIAMACHY) (Burrows et al., 1995; Bovensmann et al., 1999), the second Global Ozone Monitoring Experiment (GOME-2) (Callies et al., 2000), and the Ozone Monitoring Instrument (OMI) (Levelt et al., 2006) have been used to retrieve global maps of CHOCHO distribution by applying the Differential Optical Absorption Spectroscopy (DOAS) method (Platt and Stutz, 2008) in the visible spectral region. Wittrock et al. (2006) have first derived the distribution of CHOCHO vertical columns from SCIAMACHY observations whilst a few years later, Vrekoussis et al. (2009) presented a long-term study of its spatial and temporal variability. One year later, Vrekoussis et al. (2010) and Lerot et al. (2010) reported on the first GOME-2 retrievals of CHOCHO columns. Vrekoussis et al. (2010) used the ratio of collocated CHOCHO and HCHO vertical columns to classify various VOC sources, whereas Lerot et al. (2010) presented for the first time a retrieval algorithm with a two-step approach to reduce interferences in the CHOCHO analysis over some oceanic regions caused by liquid water absorption. The latter approach resulted in an improvement of the fit quality and less negative CHOCHO columns over clear water regions. Kurosu et al. (2007) presented a first glyoxal product based on OMI data and compared global maps for different seasons. All studies showed that glyoxal can have high values over tropical and sub-tropical regions, mainly over regions with

AMTD
7, 5559–5599, 2014

biomass burning and biogenic activities. In addition, several hot-spots were identified over areas of anthropogenic activities and over tropical oceans, the latter suggesting a potential "unknown" source of CHOCHO.

In the present study, results of an improved CHOCHO DOAS retrieval applied to the radiances measured by the OMI instrument are presented. Sensitivity tests have been performed aiming at the optimization of the CHOCHO retrieval parameters, and at reducing spectral interferences with liquid water absorption over ocean regions and with tropospheric NO_2 absorption over areas with large NO_x emissions.

Section 2 of the paper includes a description of the satellite instrument, the retrieval approach used to obtain the atmospheric CHOCHO columns including sensitivity analysis, as well as a description of the interferences with liquid water absorption over ocean and with NO_2 absorption over regions with large NO_x emissions. Section 3 presents a detailed comparison of the annual cycle of the glyoxal vertical columns, retrieved with the new OMI algorithm, with SCIAMACHY and GOME-2 glyoxal products over selected regions of interest. In Sect. 4, seasonal maps of OMI glyoxal are presented. In the last section, the OMI glyoxal product is used to investigate the link between CHOCHO columns and biomass burning in Africa as well as during the massive fire event close to Moscow in 2010.

2 Methods

2.1 The OMI instrument

The Ozone Monitoring Instrument on board NASA's Aura satellite is a nadir viewing imaging spectrograph that measures backscattered radiation in the wavelength range from 270 to 500 nm with a spectral resolution between 0.42 and 0.63 nm and a spectral sampling of between 0.15 and 0.32 nm. The instrument's spatial resolution is 13 km × 24 km at nadir and towards the scan edges the pixels become significantly

AMTD
7, 5559–5599, 2014

larger across-track. OMI has a swath that provides global coverage in one day (14 orbits) (Levelt et al., 2006), and has been recording data since October 2004.

2.2 Glyoxal retrieval

The DOAS method, based on absorption spectroscopy, allows the determination of atmospheric amounts of trace gases with narrow absorption bands in the ultraviolet (UV) and visible regions of the electromagnetic spectrum. The method analyses the intensity of the absorption bands using the Beer–Lambert law (Platt and Stutz, 2008, and references therein). The DOAS technique is based on the separation of high and low frequency variations in the absorption spectrum (optical depth spectra). The latter, together with Rayleigh and Mie scattering, are removed by a polynomial in wavelength. The narrow absorption bands are used to retrieve the trace gas slant column densities (SCs) by taking into account the absorption cross sections of all relevant trace gases. SCs represent the amount of the absorbing trace gas integrated along the effective light path in the atmosphere and can be determined by a non linear least-squares method.

For the retrieval of weak absorbers such as CHOCHO, an appropriate selection of the fitting window is a prerequisite for achieving a good DOAS fit. Most retrievals focus on avoiding spectral regions where interfering species have significant absorption lines. Retrievals of CHOCHO are usually performed in the spectral window between 420 and 460 nm and including different interference species (see Sect. 2.3), as well as a polynomial of order 2, 3 or 4 for the removal of broad band signatures (Wittrock et al., 2006; Vrekoussis et al., 2009) are included. As mentioned above, Lerot et al. (2010) showed that absorption by liquid water interferes with CHOCHO retrievals over oceans, and a pre-fitting of the liquid water signature using a larger fitting window was suggested to improve the CHOCHO retrievals. Despite these efforts to achieve better CHOCHO retrievals, the results are still affected by large uncertainties. Here, we present a new retrieval for data of the OMI instrument based on detailed sensitivity tests.

The settings used in the glyoxal retrievals within this study are described in detailed below.

AMTD
7, 5559–5599, 2014

2.3 Reference absorption cross sections

The reference absorption cross sections used in the retrieval include CHOCHO (Volkamer et al., 2005b) as well as the interfering species. In the wavelength range of 420–460 nm, interferences with O_3 (Bogumil et al., 2003), NO_2 (Vandaele et al., 1998), O_4 (Thalman and Volkamer, 2013), water vapour (Rothman et al., 2005), and liquid water (Pope and Fry, 1997) can be found. Moreover, a synthetic ring spectrum (Vountas et al., 1998) accounting for the Ring effect is included. All absorption cross sections were convoluted to OMI's spectral resolution taking into account the variation of slit function across the CCD.

2.4 Dependence on the fitting window

Systematic errors can be introduced into the glyoxal retrieval by possible cross correlations between reference cross-sections, by the influence of instrumental features, and by shifts in the wavelength calibration. Thus, a dependence on the fitting window can be observed in the retrieved CHOCHO SCs, because all these systematic errors exhibit a dependency on the wavelength interval.

In order to test the sensitivity of the retrieval on the wavelength interval selected and to find an optimal fitting window for the CHOCHO retrieval, a synthetic measurement spectrum of backscattered Earthshine was computed using the radiative transfer model SCIATRAN (Rozanov et al., 2013). A satellite measurement in nadir geometry, at solar zenith angle of 41° and constant surface reflectance of 5 % was simulated in the wavelength range of 365–500 nm at a spectral sampling of 0.2 nm. Absorption cross-sections of CHOCHO and interfering species, degraded to the OMI resolution, are used to model absorption processes in the light path. For the atmospheric profiles, the assumption of a CHOCHO concentration profile, exponentially decreasing with altitude, and no stratospheric contribution was made. The sensitivity test consists of retrievals of glyoxal SCs in different wavelength intervals. The results are shown in Fig. 1 (top), where each pixel corresponds to one CHOCHO SC retrieved using one

AMTD
7, 5559–5599, 2014

particular wavelength range and is colour coded according to the relative difference between the retrieved and a-priori SCs. The wavelength intervals have start limits of 420–437 nm, end limits of 442–460 nm, and the limits have steps of 0.2 nm. This test follows the method developed in Vogel et al. (2013).

The observed deviations are mostly rather small (i.e., $< 4\,\%$); the most accurate retrievals are found in the wavelength intervals with start limits of 430–436 nm and end limits of 456–460 nm. This wavelength range corresponds to the strongest glyoxal absorption. In Fig. 1 (bottom), the blue lines mark the start limits and the green lines the end limits for these optimal wavelength intervals.

To contrast these results with real data, a similar test was performed for selected relatively small areas over Africa, Europe, North America (N-Am.), Brazil, a desert region, and an oceanic area (see Table 1). These regions were selected to be representative for different CHOCHO levels and sources as well as possible interfering effects (sand, liquid water absorption). For each region, more than 1.0×10^2 spectra were included to obtain significant results and to limit the effect of measurement noise. The retrieval settings were identical to the synthetic test described above; additionally, an intensity offset was included. Figure 2 shows averages of the retrieved SCs for each region and for all wavelength ranges. The variation in retrieved SCs is large on real data for all regions selected, highlighting the fact that glyoxal retrievals are very sensitive to details of the fitting parameters selected. Similar variability in the results is found for ground-based data and retrievals on SCIAMACHY and GOME-2 data (not shown), but the observed pattern of deviations varies. This indicates that both interference between absorption from different absorbers and also instrumental effects may play a role. In the absence of validation data, the true columns are not known for the test on real data. However, some consistency considerations can help to make a choice for the optimal fitting range. For Africa, Brazil, and Europe, the SC means are almost homogeneous for wavelength intervals with start limits of 432–436 nm and end limits of 456–460 nm, which is consistent with the findings from the synthetic spectrum. Moreover, the desert region shows mean values close to zero within these wavelength limits,

AMTD
7, 5559–5599, 2014

which is realistic because under normal circumstances, no CHOCHO can be expected in the desert atmosphere. However, over the ocean region, negative SC means are obtained, probably as a consequence of interference with liquid water absorption (Lerot et al., 2010).

In the following, we will therefore use a fitting window extending from 433 to 458 nm, as indicated by the shaded area in Fig. 1 (bottom). This wavelength range covers the strong CHOCHO absorption bands, which have already been used to retrieve glyoxal from ground-based and ship-based instruments (Sinreich et al., 2007, 2010) as well as from satellite data (Wittrock et al., 2006; Vrekoussis et al., 2009, 2010; Lerot et al., 2010).

2.5 Dependence on the polynomial order

Another main parameter in the DOAS retrieval is the order of the polynomial accounting for the broadband features in the measured spectra. Experience shows that a low order polynomial helps to avoid instability in the fit, while increasing the degree usually improves the fitting residual, in particular for large fitting windows. In order to evaluate the dependence of the fit results on the polynomial degree, the glyoxal retrievals were performed for both cases (i.e., using the synthetic spectrum and real data) for polynomial orders 2, 3, and 4. For the synthetic spectrum, Fig. 3 (top) shows the deviation of the CHOCHO SCs from the a-priori, for polynomial degrees 2, 3, and 4. The results are similar for polynomial orders 3 and 4, however the SCs retrieved with polynomial order 2 show a relatively large deviation from the true value for most wavelength intervals. For comparison, the glyoxal columns from the real OMI measurements over a small region in Africa have also been retrieved for August 2007 as high glyoxal levels are expected over this area in summer due to biogenic activity and biomass burning. Figure 3 (bottom) shows similar patterns for polynomial orders 3 and 4, while polynomial degree 2 yields lower CHOCHO SCs in the wavelength area of interest (433–458 nm). Thus, in order to keep the degrees of freedom in the retrieval low, a polynomial order of 3 is used.

AMTD
7, 5559–5599, 2014

2.6 Interference with liquid water absorption

One of the main problems in glyoxal retrievals found by Vrekoussis et al. (2009) was the negative CHOCHO SC values over the remote Pacific Ocean, possibly due to interferences with the absorption by liquid water. Later, similar results were found by Lerot et al. (2010); they proposed a two-step retrieval to reduce the negative values over ocean regions. In a first step, they retrieved liquid water SCs from a large fitting window (405–490 nm). In a second step, they then retrieved glyoxal SCs in the wavelength range of 435–460 nm, fixing the liquid water SC to the results from the first step. This method worked well for GOME-2 fits, significantly reducing the impact of liquid water absorption on the glyoxal fits. Similar problems of interferences over ocean regions were found in the glyoxal retrieval from OMI measurements.

In order to reduce the number of negative glyoxal SCs over the remote Pacific Ocean, two different approaches were tested. First, we followed the approach by Lerot et al. (2010) and introduced a two-step fitting procedure, where the absorption by liquid water is determined in a pre-fit using a wavelength range of 410–495 nm. However, the two-step approach was only applied over water bodies, as no liquid water interferences are expected over land. In a second test, a liquid water absorption cross section was introduced in the standard DOAS fit for measurements over ocean regions. Figure 4 shows a comparison of the monthly global maps of CHOCHO SCs for August 2007 (top), and the CHOCHO SC means retrieved over a small oceanic region (latitude: 25.0° ± 1.0°; longitude: 144.0° ± 1.0°) for different wavelength intervals (bottom).

All three maps show a similar pattern over ocean with negative values over clear water regions but the amplitude varies. Clearly, SCs obtained from the standard retrieval without liquid water absorption cross section have more negative results over oceans than the two retrievals that add this cross-section. As can be seen from the maps showing the dependence on fitting window, the introduction of the liquid water correction has large effects in all windows and greatly reduces the areas with negative

AMTD
7, 5559–5599, 2014

results. In the fitting region identified as optimal in earlier tests, the retrievals over the ocean are close to 0 when including the liquid water cross-section. The smallest number of negative values is obtained when including the liquid water cross-section directly in the fit, and therefore this option was selected for the final data product.

Although the CHOCHO SCs retrieved by including the liquid water cross-section are improved over the oceans, the interference with liquid water is still present to a lesser degree, judging from the fact that some regions with negative CHOCHO SC values still remain. Whether this is the result of non optimal cross-sections for liquid water (Peters et al., 2014) or other effects such as vibrational Raman scattering in the ocean cannot be decided at this point.

2.7 Interference with NO_2 absorption

Some urban and industrial regions show high levels of glyoxal (e.g., the large urban agglomerations Johannesburg, Los Angeles, Beijing, and Guangzhou) due to the production of CHOCHO from aromatics and acetylene (Volkamer et al., 2007; Myriokefalitakis et al., 2008; Liu et al., 2012). However, the observed signal could potentially also be influenced by spectral interferences with tropospheric NO_2 which is very abundant in these regions (see Fig. 5, top). To test this, an additional NO_2 absorption cross-section measured at high temperature (i.e., typical surface, 298 K) was included in the glyoxal retrieval to better represent near-surface NO_2.

Monthly maps of glyoxal SCs for September 2007 are shown in Fig. 5. Including the high temperature NO_2 absorption cross-section in the fit leads to decreased glyoxal SC values over pollution hot-spots and improves the fitting residuals. The improvement of chisquare values over these regions is up to 5 % and even large in some cases. However, glyoxal values still remain high in all cases, indicating that the observed enhancements are not artefacts but rather indicate genuine anthropogenic sources.

To further investigate the effect of including the high temperature cross-section of NO_2, a comparison between the glyoxal seasonal variation including and excluding

AMTD
7, 5559–5599, 2014

the term is presented in Fig. 6 (top) for the regions of Beijing (latitude: 37.5° ± 2.5°; longitude: 115.5° ± 1.5°) and Congo (latitude: −4.0° ± 2.0°; longitude: 18.0° ± 2.0°).

The results show similar seasonal variability, however there are large differences (up to 25 %) observed during winter especially in Beijing where the anthropogenic emissions of NO_x are higher than in Congo (see Fig. 6, bottom), because the latter is mainly influenced by biogenic emissions and fires. This result underlines the fact that there appears to be an interference from large tropospheric NO_2 columns in the gloxal retrieval which also impacts on the seasonality over polluted regions.

2.8 Air mass factor computation

As the SC depends on observation geometry, it is often useful to compute the vertical column which is defined as $VC = \int \rho_i(z) dz$, where $\rho_i(z)$ is the concentration of the species and dz is the vertical path through the atmosphere.

The vertical and slant columns are related by the air mass factor (AMF). The AMF is defined as the ratio of SC and VC and depends on the radiative transfer in the atmosphere (Platt and Stutz, 2008). It depends on the trace gas profile, air pressure, surface albedo, temperature, ozone and aerosol profiles, clouds, as well as on the SZA and the measurement geometry.

In this work, the AMFs have been calculated by the radiative transfer model SCIATRAN (Rozanov et al., 2005) assuming typical glyoxal profiles as is described in Wittrock (2006). More sophisticated a priori data including aerosol and cloud effects are needed in the future, but improvements of AMFs are not the focus of the present study.

2.9 Glyoxal detection limit and error

When investigating the uncertainty of the retrieved glyoxal columns, several effects have to be taken into account. Photon-shot noise, related to the number of photons collected in a single measurement and governed by the probability distribution of incoming photons (Burrows et al., 2011), together with readout noise and the dark signal

AMTD
7, 5559–5599, 2014

in the detector, are the main sources of random errors in the radiance measurements. Systematic errors in the slant columns are introduced by uncertainties in reference spectra, an imperfect wavelength calibration, and instrumental features. These, combined with other parameters such as the limited penetration of solar radiation due the scattering effects in the atmosphere, determine the total uncertainty of the retrieved glyoxal SCs.

When discussing vertical columns, the vertical profiles and climatology used in the air mass factor calculations introduce additional uncertainties in the results. Moreover, the surface reflectance is important for the air mass factor computation, and any uncertainty in that will impact on the accuracy of the vertical columns.

Furthermore, the influence of clouds and aerosols on the glyoxal retrievals from satellite observations is high (Vrekoussis et al., 2009). As clouds are highly reflective and usually above the tropospheric pollution layer (e.g., in biomass burning regions), they have significant effects on satellite observations (Wang et al., 2008).

The systematic errors in the glyoxal retrievals are considered to be approximately constant over time and can introduce large offsets in the results. In this study, in order to account for these effects, the normalization method of columns introduced in Vrekoussis et al. (2009) has been applied, which consists in computing the mean of the slant columns over an area in the remote Pacific Ocean (lat.: $0^\circ \pm 60^\circ$; long.: $180^\circ \pm 30^\circ$), and subtracting this value from all the measurements of the same day. In order to account for the glyoxal background, a vertical column of 2.0×10^{14} molec cm^{-2} is then added to the global field.

For the computation of the detection limit, the minimum glyoxal slant columns detectable with the DOAS retrieval from OMI measurements are estimated for an ideal case of a single measurement. This detection limit is given by the ratio between the root mean square (RMS) at the residual and the maximum differential absorption cross section of the trace gas of interest (σ_{CHOCHO}). The typical RMS for a single measurement in a region where high glyoxal amounts are found (e.g. Africa) is around 6×10^{-4} and the maximum of the CHOCHO absorption cross section is 5.5×10^{-19} cm^2 molec^{-1}.

AMTD
7, 5559–5599, 2014

Thus, the SC detection limit for the ideal case and a single measurement is around of 1.0×10^{15} molec cm^{-2}. This limit is reduced by averaging over time or space.

For comparison, the scatter of SCs over a clean region in the equatorial Pacific (5° S–5° N, 160–200° E) has been computed for August 2007. As illustrated in Fig. 7, the SC scatter shows a distribution around zero with FWHM of 3.3×10^{15} molec cm^{-2} and a standard deviation of 1.4×10^{15} molec cm^{-2}, which is of the same order of magnitude as obtained for the detection limit.

3 Comparison to GOME-2 and SCIAMACHY data

In order to evaluate the quality and consistency of the improved OMI glyoxal retrieval, a comparison with GOME-2 and SCIAMACHY data has been performed using similar fitting parameters for all data sets. The only exception is the polynomial order used, which had to be adapted for each instrument most likely due to the different instrumental effects. Moreover, no liquid water correction is applied to the SCIAMACHY and GOME-2 retrievals. We therefore focus the comparison between instrument on measurements over land. Table 2 summarizes the main fitting parameters used in the glyoxal retrievals from OMI, GOME-2, and SCIAMACHY.

In order to take into account the influence of clouds on the OMI CHOCHO retrievals, a cloud screening is applied based on the OMI O_4 cloud product (Acarreta et al., 2004) using a cloud threshold of 30 %. For GOME-2 and SCIAMACHY a cloud correction based on FRESCO+ cloud screening is applied (Wang et al., 2008). Moreover, a destriping correction is needed in the OMI CHOCHO retrieval in order to remove the stripes generated by instrumental effects.

For this comparison, we used monthly mean VCs from the GOME-2 and SCIAMACHY instruments. Briefly, SCIAMACHY and GOME-2 are nadir viewing spectrometers providing the spectral coverage and resolution needed for DOAS retrievals of atmospheric trace gases. These instruments measure the light scattered by the atmosphere in the UV and visible range. They have a spatial resolution of 60 km × 30 km and

AMTD
7, 5559–5599, 2014

80 km × 40 km, respectively. SCIAMACHY had an equator crossing time of 10:00 LT, and global coverage was achieved in six days, while GOME-2 has a nearly daily global coverage and an equatorial overpass time of 09:30 LT (Burrows et al., 1995; Bovensmann et al., 1999; Callies et al., 2000).

In Fig. 8 (top), time series of monthly mean CHOCHO VCs over twelve regions (see Table 3) are shown for 2007. The monthly observations are averaged within each of the areas, which represent different environments with large glyoxal production from biogenic, anthropogenic, and pyrogenic sources (see Fig. 8, bottom). The seasonal variabilities of the data sets have an overall good consistency. At closer inspection, good agreement is found in the temporal behaviour among data sets over regions dominated by biogenic emissions and also with large anthropogenic activities, such as China (South and East). However, SCIAMACHY data are often higher than OMI and GOME-2 results. Also, the temporal variability of glyoxal over Africa and South America is less pronounced than in North America and Australia, which is possibly related to large constant emissions of vegetation in those areas.

4 Seasonal variation

In order to study the seasonal variability of CHOCHO, average maps of CHOCHO VCs for northern hemispheric winter (DJF), spring (MAM), summer (JJA), and autumn (SON) are presented in Fig. 9. These are averaged for the respective seasons within the time period 2005 to 2013. The maps show that the highest levels of CHOCHO are found in the tropical and sub-tropical regions. The CHOCHO VCs vary with the season, the maxima and minima corresponding to the respective summer and winter. This is consistent with the fact that the biogenic emissions increase in the warm periods and thus the CHOCHO production is enhanced. Whereas the largest CHOCHO amounts are found in Africa north of the equator in winter, the maximum in CHOCHO production due to fire emissions is observed in summer over central Africa. Moreover, the maximum of CHOCHO in South America corresponds to autumn, in agreement

AMTD
7, 5559–5599, 2014

with the largest fire activity and the highest NO_2 levels during that part of the season (Schreier et al., 2014). Close to the equator, the CHOCHO seasonal variation is quite smooth, suggesting that the CHOCHO is mostly produced by biogenic sources from tropical forests (Guenther et al., 2006). In contrast, CHOCHO from biogenic sources at higher latitudes has a clear seasonal cycle with the maximum in summer (e.g., Southeast US), which corresponds to the vegetation growth cycle. Additionally, no significant differences were found between seasons over anthropogenic regions (e.g., Southeast China), most likely as result of different sources contributing to the CHOCHO amounts in the different seasons (e.g., anthropogenic emissions in winter, biogenic production in spring).

5 Glyoxal as an indicator of pyrogenic emissions

Pyrogenic emission is one of the main sources of trace gases in the atmosphere and is estimated to contribute 18 % of the global CHOCHO levels released to the atmosphere (Stavrakou et al., 2009a). Around 60 % of this are emitted directly by the fires and the rest by secondary production. Moreover, it is well known that large fire events occur during the warm season and mainly over continental Africa. In order to identify the regions with largest production of CHOCHO over Africa, correlation coefficients between CHOCHO VCs and fire radiative power (FRP) are presented. FRP is a measure of outgoing radiant heat from fires (in units of Watt), which can be retrieved from the MODerate resolution Imaging Spectroradiometers (MODIS) on board NASA's Terra and Aqua satellites (Justice et al., 2002). Additionally, CHOCHO columns are used to investigate the effect of a large fire event close to Moscow in 2010.

5.1 Correlation with fires over Africa

The correlation coefficients are determined by assuming a linear relationship between CHOCHO VCs and FRP for the African continent and are illustrated in Fig. 10 (left). The

AMTD
7, 5559–5599, 2014

calculations were performed with a grid resolution of 0.5° × 0.5° using monthly means of OMI CHOCHO VCs and FRP from MODIS on board Aqua (MYD14CMH) (Justice et al., 2002). A linear relationship between tropospheric NO_2 VCs and FRP was already showed by Schreier et al. (2014). They demonstrated a strong link between the seasonal cycles of tropospheric NO_2 and FRP for the main biomass burning regions. In this study, we found a comparable connection between CHOCHO and FRP for two similar regions in Africa as shown in Schreier et al. (2014). The time series of spatially averaged monthly means are show in Fig. 10 (right) for the two regions. Although pyrogenic emissions contribute only about 18 % to the global budget of CHOCHO (Stavrakou et al., 2009a), there clearly exist some regions where fires are the dominant source of glyoxal and where good agreement in seasonal behaviour is found with FRP. Moreover, additional peaks are observed in CHOCHO VCs during the wet season in both regions. As there is no significant fire activity during this part of season, these peaks are most likely caused by biogenic sources.

5.2 Russian fires in 2010

In summer 2010, unprecedented temperature anomalies causing severe drought in some areas of European Russia resulted in the outbreak of many wildfires (Shvidenko et al., 2011). Beginning in mid-July, the number of fires showed a steadily increasing occurrence until the end days of July, followed by a decrease in August (Parshutkina et al., 2011).

The wildfires around Moscow created elevated atmospheric levels of carbon monoxide (CO), NO_x, O_3, sulfur dioxide (SO_2), methane (CH_4), carbon dioxide (CO_2), ammonia (NH_3), formic acid (HCOOH), and aerosol load, affecting air quality and human health (Yurganov et al., 2011; Elansky et al., 2011; Konovalov et al., 2011; van Donkelaar et al., 2011; R'Honi et al., 2013). Here, we show that high levels of glyoxal have also been produced from these wildfires.

For this case study, we use the 24 h assimilation data of FRP from the Global Fire Assimilation System (GFASv1.0) (Kaiser et al., 2012). Briefly, GFASv1.0 spatially

AMTD
7, 5559–5599, 2014

aggregates all valid observations of fire and non-fire from the two MODIS instruments onto a horizontal resolution of 0.5°×0.5° and calculates the total FRP sums for each grid cell. Further details about the daily 24 h assimilated GFASv1.0 FRP product, which we use for the following analysis of Russian wildfires can be found in Kaiser et al. (2012).

The geographical distribution of the 24 h assimilated FRP and the tropospheric vertical columns of CHOCHO are shown in Fig. 11 for the period 22 July to 18 August 2010, which represents the main part of the fire period. The largest fire activity is observed in the east of Moscow, which is in excellent agreement with the location where highest CHOCHO VCs are found. This is a clear indication of glyoxal emissions from forest fires. Another hot-spot of fire activity during the selected time period is observed between 60° and 65° N and 60° and 65° E. However, these fires are much less intense, and thus, the magnitude of the observed CHOCHO columns is lower.

6 Summary and conlusions

In this study, an improved glyoxal product has been developed for OMI measurements, expanding the data set available from SCIAMACHY and GOME-2 to data taken in an afternoon orbit. Sensitivity tests on synthetic data as well as on OMI measurements over selected regions provided useful information for the optimization of DOAS fitting window and the selection of optimal polynomial degree for this study. Moreover, two approaches for the reduction of the liquid water interference over clear water oceans have been evaluated, finding that including the liquid water absorption cross-section in the DOAS fit leads to the best reduction of negative glyoxal values over oceans, at least in the OMI data. For the first time, possible interferences by tropospheric NO_2 over areas with large anthropogenic emissions has been investigated. A high temperature NO_2 absorption cross-section representing near-surface NO_2 has been introduced in the retrieval, leading to a significant reduction of glyoxal over these areas at high NO_2 and improved fit quality.

AMTD
7, 5559–5599, 2014

The comparison of OMI glyoxal with GOME-2 and SCIAMACHY data shows good overall agreement over areas with large biogenic emissions. Significant differences were found over regions with large anthropogenic emissions. Moreover, a similar seasonal behaviour is observed among the three products.

The new CHOCHO retrieval has been applied to identify pyrogenic activities over Africa and for the large Russian wildfire during August 2010. It was shown that the location and temporal pattern of the retrieved glyoxal columns is closely linked with the fire radiative power observations, indicating that in these areas, pyrogenic emissions dominate the glyoxal signal.

In spite of the progress made on OMI glyoxal retrieval here, the resulting data sets are still noisy and depend critically on the details of the selections made for the retrieval. Further improvements in signal to noise and consistency are needed to make full use of the synergy between measurements from instrument in morning and afternoon orbits. In addition, the effects of clouds and aerosols on the air mass factors need to be taken into account, in particular for biomass burning scenarios.

Acknowledgements. Leonardo Alvarado gratefully acknowledges funding by the German Academic Exchange Service (DAAD). We acknowledge financial support provided by the University of Bremen and the Earth System Science Research School (ESSReS), an initiative of the Helmholtz Association of German Research Centres (HGF) at the Alfred Wegener Institute for Polar and Marine Research (AWI). We want to thank Johannes Kaiser and the MACC team for providing the GFASv1.0 FRP product as well as Michel Van Roozendael for helpful comments and suggestions. OMI lv1 data have been provided by NASA. GOME-2 lv1 data have been provided by EUMETSAT. SCIAMACHY lv1 data have been provided by ESA through DLR.

References

Acarreta, J. R., De Haan, J. F., and Stammes, P.: Cloud pressure retrieval using the O_2-O_2 absorption band at 477 nm, J. Geophys. Res.-Atmos., 109, D05204, doi:10.1029/2003JD003915, 2004. 5572

AMTD
7, 5559–5599, 2014

Andreae, M. O. and Merlet, P.: Emission of trace gases and aerosols from biomass burning, Global Biogeochem. Cy., 15, 955–966, doi:10.1029/2000GB001382, 2001. 5561
Atkinson, R.: Atmospheric chemistry of VOCs and NO_x, Atmos. Environ., 34, 2063–2101, doi:10.1016/S1352-2310(99)00460-4, 2000. 5562
Atkinson, R. and Arey, J.: Gas-phase tropospheric chemistry of biogenic volatile organic compounds: a review, Atmos. Environ., 37, Supplement 2, 197–219, doi:10.1016/S1352-2310(03)00391-1, 2003. 5561
Bogumil, K., Orphal, J., Homann, T., Voigt, S., Spietz, P., Fleischmann, O., Vogel, A., Hartmann, M., Kromminga, H., Bovensmann, H., Frerick, J., and Burrows, J.: Measurements of molecular absorption spectra with the SCIAMACHY pre-flight model: instrument characterization and reference data for atmospheric remote-sensing in the 230–2380 nm region, J. Photochem. Photobiol. A, 157, 167–184, doi:10.1016/S1010-6030(03)00062-5, 2003. 5565
Bovensmann, H., Burrows, J. P., Buchwitz, M., Frerick, J., Noël, S., Rozanov, V. V., Chance, K. V., and Goede, A. P. H.: SCIAMACHY: mission objectives and measurement modes, J. Atmos. Sci., 56, 127–150, doi:10.1175/1520-0469(1999)056<0127:SMOAMM>2.0.CO;2, 1999. 5562, 5573
Burrows, J., Hölzle, E., Goede, A., Visser, H., and Fricke, W.: SCIAMACHY – scanning imaging absorption spectrometer for atmospheric chartography, Acta Astronaut., 35, 445–451, doi:10.1016/0094-5765(94)00278-T, 1995. 5562, 5573
Burrows, J. P., Platt, U., and Borrell, P.: Tropospheric Remote Sensing from Space, in: The Remote Sensing of Tropospheric Composition from Space, edited by: Burrows, J. P., Borrell, P., Platt, U., Guzzi, R., Platt, U., and Lanzerotti, L. J.: Physics of Earth and Space Environments, Springer, Berlin, Heidelberg, 1–65, 2011. 5570
Callies, J., Corpaccioli, E., Eisinger, M., Hahne, A., and Lefebvre, A.: GOME-2 – Metop's second-generation sensor for operational ozone monitoring, ESA Bulletin, 102, 28–36, 2000. 5562, 5573
Curci, G., Palmer, P. I., Kurosu, T. P., Chance, K., and Visconti, G.: Estimating European volatile organic compound emissions using satellite observations of formaldehyde from the Ozone Monitoring Instrument, Atmos. Chem. Phys., 10, 11501–11517, doi:10.5194/acp-10-11501-2010, 2010. 5561
Elansky, N. F., Mokhov, I. I., Belikov, I. B., Berezina, E. V., Elokhov, A. S., Ivanov, V. A., Pankratova, N. V., Postylyakov, O. V., Safronov, A. N., Skorokhod, A. I., and Shumskii, R. A.:

AMTD
7, 5559–5599, 2014

Gaseous admixtures in the atmosphere over Moscow during the 2010 summer, Izvestiya, Atmos. Ocean. Phys., 47, 672–681, doi:10.1134/S000143381106003X, 2011. 5575
Fu, T.-M., Jacob, D. J., Wittrock, F., Burrows, J. P., Vrekoussis, M., and Henze, D. K.: Global budgets of atmospheric glyoxal and methylglyoxal, and implications for formation of secondary organic aerosols, J. Geophys. Res.-Atmos., 113, D15303, doi:10.1029/2007JD009505, 2008. 5561, 5562
Guenther, A., Hewitt, C. N., Erickson, D., Fall, R., Geron, C., Graedel, T., Harley, P., Klinger, L., Lerdau, M., Mckay, W. A., Pierce, T., Scholes, B., Steinbrecher, R., Tallamraju, R., Taylor, J., and Zimmerman, P.: A global model of natural volatile organic compound emissions, J. Geophys. Res.-Atmos., 100, 8873–8892, doi:10.1029/94JD02950, 1995. 5561
Guenther, A., Geron, C., Pierce, T., Lamb, B., Harley, P., and Fall, R.: Natural emissions of non-methane volatile organic compounds, carbon monoxide, and oxides of nitrogen from North America, Atmos. Environ., 34, 2205–2230, doi:10.1016/S1352-2310(99)00465-3, 2000. 5561
Guenther, A., Karl, T., Harley, P., Wiedinmyer, C., Palmer, P. I., and Geron, C.: Estimates of global terrestrial isoprene emissions using MEGAN (Model of Emissions of Gases and Aerosols from Nature), Atmos. Chem. Phys., 6, 3181–3210, doi:10.5194/acp-6-3181-2006, 2006. 5574
Houweling, S., Dentener, F., and Lelieveld, J.: The impact of nonmethane hydrocarbon compounds on tropospheric photochemistry, J. Geophys. Res.-Atmos., 103, 10673–10696, doi:10.1029/97JD03582, 1998. 5561
Justice, C., Giglio, L., Korontzi, S., Owens, J., Morisette, J., Roy, D., Descloitres, J., Alleaume, S., Petitcolin, F., and Kaufman, Y.: The MODIS fire products, Remote Sens. Environ., 83, 244–262, doi:10.1016/S0034-4257(02)00076-7, 2002. 5574, 5575
Kaiser, J. W., Heil, A., Andreae, M. O., Benedetti, A., Chubarova, N., Jones, L., Morcrette, J.-J., Razinger, M., Schultz, M. G., Suttie, M., and van der Werf, G. R.: Biomass burning emissions estimated with a global fire assimilation system based on observed fire radiative power, Biogeosciences, 9, 527–554, doi:10.5194/bg-9-527-2012, 2012. 5575, 5576
Kansal, A.: Sources and reactivity of NMHCs and VOCs in the atmosphere: a review, J. Hazard. Mater., 166, 17–26, doi:10.1016/j.jhazmat.2008.11.048, 2009. 5561
Konovalov, I. B., Beekmann, M., Kuznetsova, I. N., Yurova, A., and Zvyagintsev, A. M.: Atmospheric impacts of the 2010 Russian wildfires: integrating modelling and measurements of an

AMTD
7, 5559–5599, 2014

extreme air pollution episode in the Moscow region, Atmos. Chem. Phys., 11, 10031–10056, doi:10.5194/acp-11-10031-2011, 2011. 5575
Kurosu, T. P., Chance, K., Liu, X., Volkamer, R., Fu, T.-M., Millet, D., and Jacob, D. J.: Seasonally resolved global distributions of glyoxal and formaldehyde observed from the Ozone Monitoring Instrument on EOS Aura, in: Proceeding of Anais XIII Simpósio Brasileiro de Sensoriamento Remoto, 2007. 5562
Lerot, C., Stavrakou, T., De Smedt, I., Müller, J.-F., and Van Roozendael, M.: Glyoxal vertical columns from GOME-2 backscattered light measurements and comparisons with a global model, Atmos. Chem. Phys., 10, 12059–12072, doi:10.5194/acp-10-12059-2010, 2010. 5562, 5564, 5567, 5568
Levelt, P., van den Oord, G., Dobber, M., Malkki, A., Visser, H., Vries, J. d., Stammes, P., Lundell, J., and Saari, H.: The ozone monitoring instrument, IEEE T. Geosci. Remote, 44, 1093–1101, doi:10.1109/TGRS.2006.872333, 2006. 5562, 5564
Liu, Z., Wang, Y., Vrekoussis, M., Richter, A., Wittrock, F., Burrows, J. P., Shao, M., Chang, C.-C., Liu, S.-C., Wang, H., and Chen, C.: Exploring the missing source of glyoxal (CHOCHO) over China, Geophys. Res. Lett., 39, L10812, doi:10.1029/2012GL051645, 2012. 5562, 5569
Myriokefalitakis, S., Vrekoussis, M., Tsigaridis, K., Wittrock, F., Richter, A., Brühl, C., Volkamer, R., Burrows, J. P., and Kanakidou, M.: The influence of natural and anthropogenic secondary sources on the glyoxal global distribution, Atmos. Chem. Phys., 8, 4965–4981, doi:10.5194/acp-8-4965-2008, 2008. 5561, 5569
Parshutkina, I. P., Sosnikova, E. V., Grishina, N. P., Stulov, E. A., Plaude, N. O., and Monakhova, N. A.: Atmospheric aerosol characterization in 2010 anomalous summer season in the Moscow region, Russ. Meteorol. Hydrol., 36, 355–361, doi:10.3103/S106837391106001X, 2011. 5575
Platt, U. and Stutz, J.: Differential Optical Absorption Spectroscopy: Principles and Applications, Springer, 2008. 5562, 5564, 5570
Pope, R. M. and Fry, E. S.: Absorption spectrum (380–700 nm) of pure water, II. Integrating cavity measurements, Appl. Optics, 36, 8710–8723, doi:10.1364/AO.36.008710, 1997. 5565
R'Honi, Y., Clarisse, L., Clerbaux, C., Hurtmans, D., Duflot, V., Turquety, S., Ngadi, Y., and Coheur, P.-F.: Exceptional emissions of NH_3 and HCOOH in the 2010 Russian wildfires, Atmos. Chem. Phys., 13, 4171–4181, doi:10.5194/acp-13-4171-2013, 2013. 5575
Rothman, L., Jacquemart, D., Barbe, A., Chris Benner, D., Birk, M., Brown, L., Carleer, M., Chackerian Jr., C., Chance, K., Coudert, L., Dana, V., Devi, V., Flaud, J.-M., Gamache, R.,

AMTD
7, 5559–5599, 2014

Goldman, A., Hartmann, J.-M., Jucks, K., Maki, A., Mandin, J.-Y., Massie, S., Orphal, J., Perrin, A., Rinsland, C., Smith, M., Tennyson, J., Tolchenov, R., Toth, R., Vander Auwera, J., Varanasi, P., and Wagner, G.: The HITRAN 2004 molecular spectroscopic database, J. Quant. Spectrosc. Ra., 96, 139–204, doi:10.1016/j.jqsrt.2004.10.008, 2005. 5565

Rozanov, A., Rozanov, V., Buchwitz, M., Kokhanovsky, A., and Burrows, J.: SCIATRAN 2.0 – a new radiative transfer model for geophysical applications in the 175–2400 nm spectral region, Adv. Space Res., 36, 1015–1019, doi:10.1016/j.asr.2005.03.012, 2005. 5570

Rozanov, V., Rozanov, A., Kokhanovsky, A., and Burrows, J.: Radiative transfer through terrestrial atmosphere and ocean: software package SCIATRAN, J. Quant. Spectrosc. Ra., 133, 13–71, doi:10.1016/j.jqsrt.2013.07.004, 2013. 5565

Schreier, S. F., Richter, A., Kaiser, J. W., and Burrows, J. P.: The empirical relationship between satellite-derived tropospheric NO_2 and fire radiative power and possible implications for fire emission rates of NO_x, Atmos. Chem. Phys., 14, 2447–2466, doi:10.5194/acp-14-2447-2014, 2014. 5574, 5575

Setokuchi, O.: Trajectory calculations of OH radical- and Cl atom-initiated reaction of glyoxal: atmospheric chemistry of the HC(O)CO radical, Phys. Chem. Chem. Phys., 13, 6296–6304, doi:10.1039/C0CP01942A, 2011. 5562

Shvidenko, A. Z., Shchepashchenko, D. G., Vaganov, E. A., Sukhinin, A. I., Maksyutov, S. S., McCallum, I., and Lakyda, I. P.: Impact of wildfire in Russia between 1998–2010 on ecosystems and the global carbon budget, Dokl. Earth Sci., 441, 1678–1682, doi:10.1134/S1028334X11120075, 2011. 5575

Sinreich, R., Volkamer, R., Filsinger, F., Frieß, U., Kern, C., Platt, U., Sebastián, O., and Wagner, T.: MAX-DOAS detection of glyoxal during ICARTT 2004, Atmos. Chem. Phys., 7, 1293–1303, doi:10.5194/acp-7-1293-2007, 2007. 5562, 5567

Sinreich, R., Coburn, S., Dix, B., and Volkamer, R.: Ship-based detection of glyoxal over the remote tropical Pacific Ocean, Atmos. Chem. Phys., 10, 11359–11371, doi:10.5194/acp-10-11359-2010, 2010. 5567

Stavrakou, T., Müller, J.-F., De Smedt, I., Van Roozendael, M., Kanakidou, M., Vrekoussis, M., Wittrock, F., Richter, A., and Burrows, J. P.: The continental source of glyoxal estimated by the synergistic use of spaceborne measurements and inverse modelling, Atmos. Chem. Phys., 9, 8431–8446, doi:10.5194/acp-9-8431-2009, 2009a. 5574, 5575

Stavrakou, T., Müller, J.-F., De Smedt, I., Van Roozendael, M., van der Werf, G. R., Giglio, L., and Guenther, A.: Evaluating the performance of pyrogenic and biogenic emission inven-

AMTD
7, 5559–5599, 2014

tories against one decade of space-based formaldehyde columns, Atmos. Chem. Phys., 9, 1037–1060, doi:10.5194/acp-9-1037-2009, 2009b. 5561

Tadić, J., Moortgat, G. K., and Wirtz, K.: Photolysis of glyoxal in air, J. Photoch. Photobio. A, 177, 116–124, doi:10.1016/j.jphotochem.2005.10.010, 2006. 5562

Thalman, R. and Volkamer, R.: Temperature dependent absorption cross-sections of O2–O2 collision pairs between 340 and 630 nm and at atmospherically relevant pressure, Phys. Chem. Chem. Phys., 15, 15371–15381, doi:10.1039/C3CP50968K, 2013. 5565

van Donkelaar, A., Martin, R. V., Levy, R. C., da Silva, A. M., Krzyzanowski, M., Chubarova, N. E., Semutnikova, E., and Cohen, A. J.: Satellite-based estimates of ground-level fine particulate matter during extreme events: a case study of the Moscow fires in 2010, Atmos. Environ., 45, 6225–6232, doi:10.1016/j.atmosenv.2011.07.068, 2011. 5575

Vandaele, A., Hermans, C., Simon, P., Carleer, M., Colin, R., Fally, S., Mérienne, M., Jenouvrier, A., and Coquart, B.: Measurements of the NO_2 absorption cross-section from 42 000 cm^{-1} to 10 000 cm^{-1} (238–1000 nm) at 220 K and 294 K, J. Quant. Spectrosc. Ra., 59, 171–184, doi:10.1016/S0022-4073(97)00168-4, 1998. 5565

Vogel, L., Sihler, H., Lampel, J., Wagner, T., and Platt, U.: Retrieval interval mapping: a tool to visualize the impact of the spectral retrieval range on differential optical absorption spectroscopy evaluations, Atmos. Meas. Tech., 6, 275–299, doi:10.5194/amt-6-275-2013, 2013. 5566

Volkamer, R., Molina, L. T., Molina, M. J., Shirley, T., and Brune, W. H.: DOAS measurement of glyoxal as an indicator for fast VOC chemistry in urban air, Geophys. Res. Lett., 32, L08806, doi:10.1029/2005GL022616, 2005a. 5562

Volkamer, R., Spietz, P., Burrows, J., and Platt, U.: High-resolution absorption cross-section of glyoxal in the UV–vis and IR spectral ranges, J. Photochem. Photobiol. A, 172, 35–46, doi:10.1016/j.jphotochem.2004.11.011, 2005b. 5565, 5587

Volkamer, R., San Martini, F., Molina, L. T., Salcedo, D., Jimenez, J. L., and Molina, M. J.: A missing sink for gas-phase glyoxal in Mexico City: Formation of secondary organic aerosol, Geophys. Res. Lett., 34, L19807, doi:10.1029/2007GL030752, 2007. 5562, 5569

Vountas, M., Rozanov, V., and Burrows, J.: Ring effect: impact of rotational Raman scattering on radiative transfer in earth's atmosphere, J. Quant. Spectrosc. Ra., 60, 943–961, doi:10.1016/S0022-4073(97)00186-6, 1998. 5565

AMTD
7, 5559–5599, 2014

Vrekoussis, M., Wittrock, F., Richter, A., and Burrows, J. P.: Temporal and spatial variability of glyoxal as observed from space, Atmos. Chem. Phys., 9, 4485–4504, doi:10.5194/acp-9-4485-2009, 2009. 5562, 5564, 5567, 5568, 5571

Vrekoussis, M., Wittrock, F., Richter, A., and Burrows, J. P.: GOME-2 observations of oxygenated VOCs: what can we learn from the ratio glyoxal to formaldehyde on a global scale?, Atmos. Chem. Phys., 10, 10145–10160, doi:10.5194/acp-10-10145-2010, 2010. 5561, 5562, 5567

Wang, P., Stammes, P., van der A, R., Pinardi, G., and van Roozendael, M.: FRESCO+: an improved O_2 A-band cloud retrieval algorithm for tropospheric trace gas retrievals, Atmos. Chem. Phys., 8, 6565–6576, doi:10.5194/acp-8-6565-2008, 2008. 5571, 5572

Williams, J.: Organic trace gases in the atmosphere: an overview, Environ. Chem., 1, 125–136, doi:10.1071/EN04057, 2004. 5561

Wittrock, F.: The retrieval of oxygenated volatile organic compounds by remote sensing techniques, Ph.D. thesis, University of Bremen, 2006. 5562, 5570

Wittrock, F., Richter, A., Oetjen, H., Burrows, J. P., Kanakidou, M., Myriokefalitakis, S., Volkamer, R., Beirle, S., Platt, U., and Wagner, T.: Simultaneous global observations of glyoxal and formaldehyde from space, Geophys. Res. Lett., 33, L16804, doi:10.1029/2006GL026310, 2006. 5562, 5564, 5567

Yu, S.: Role of organic acids (formic, acetic, pyruvic and oxalic) in the formation of cloud condensation nuclei (CCN): a review, Atmos. Res., 53, 185–217, doi:10.1016/S0169-8095(00)00037-5, 2000. 5561

Yurganov, L. N., Rakitin, V., Dzhola, A., August, T., Fokeeva, E., George, M., Gorchakov, G., Grechko, E., Hannon, S., Karpov, A., Ott, L., Semutnikova, E., Shumsky, R., and Strow, L.: Satellite- and ground-based CO total column observations over 2010 Russian fires: accuracy of top-down estimates based on thermal IR satellite data, Atmos. Chem. Phys., 11, 7925–7942, doi:10.5194/acp-11-7925-2011, 2011. 5575

AMTD
7, 5559–5599, 2014

Table 1. Regions selected for Fig. 2.

	Latitude [°]	Longitude [°]	Date
Africa	−5.0 ± 3.0	13.5 ± 0.5	9 Aug 2007
Brazil	−8.5 ± 3.5	−64.5 ± 2.5	19 Aug 2007
Europe	49.5 ± 3.5	7.0 ± 5.0	20 Aug 2007
N-Am.	31.0 ± 3.0	−82.5 ± 1.5	14 Aug 2007
Desert	22.0 ± 3.0	20.0 ± 4.0	15 Aug 2007
Ocean	25.0 ± 1.0	144.0 ± 1.0	1 Aug 2007

AMTD
7, 5559–5599, 2014

Table 2. Settings for the different CHOCHO retrievals.

	This work (OMI)	GOME-2	SCIAMACHY
Fitting window	433–458 nm		
Polynomial	3	4	4
Cross-sections	CHOCHO, NO_2 (220 K and 298 K), O_3 (223 K), O_4, H_2O_{vap}, Ring		
Liquid water	+	–	–

AMTD
7, 5559–5599, 2014

Table 3. Regions selected for Fig. 8.

	Box No.	Latitude [°]	Longitude [°]
N-America	1	32.0 ± 4.0	−90.0 ± 10.0
S-America-a	2	0.0 ± 10.0	−62.0 ± 8.0
S-America-b	3	−2.0 ± 4.0	−50.0 ± 3.0
W-Africa	4	6.0 ± 4.0	1.0 ± 10.0
C-Africa-a	5	2.0 ± 4.0	19.0 ± 9.0
C-Africa-b	6	−7.0 ± 5.0	19.0 ± 9.0
Indonesia	7	2.0 ± 6.0	108.0 ± 12.0
Australia	8	−14.0 ± 3.0	135.0 ± 10.0
S-China	9	25.0 ± 3.0	112.0 ± 5.0
E-China	10	34.0 ± 5.0	116.0 ± 5.0
India	11	24.0 ± 4.0	85.0 ± 7.0
Europe	12	48.0 ± 5.0	7.0 ± 6.0

AMTD
7, 5559–5599, 2014

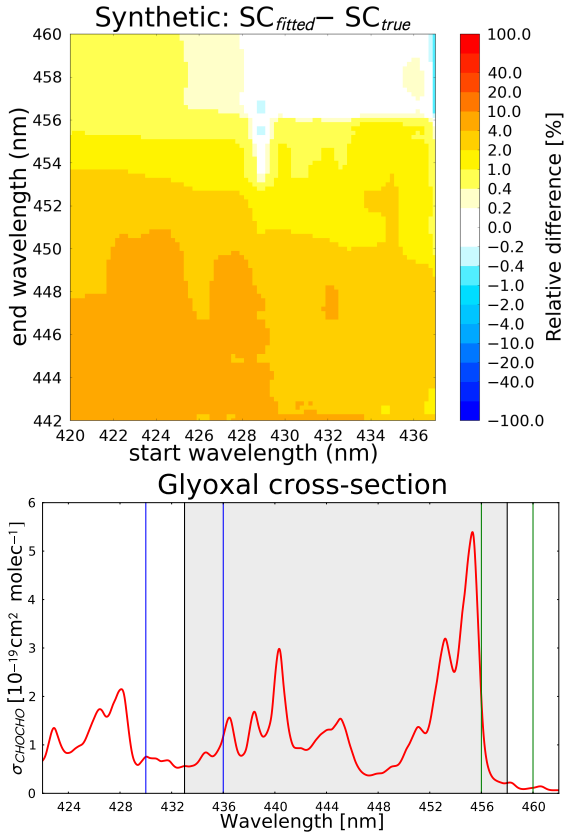

Figure 1. Colour mapping of the relative difference of CHOCHO SCs with respect to the a priori ("true value") $\left(\frac{SC_{fitted}-SC_{true}}{\frac{SC_{fitted}+SC_{true}}{2}}\right)$ retrieved from a synthetic spectrum for wavelength intervals with start limits of 420–437 nm and end limits 442–460 nm (top). Glyoxal absorption cross-section at 296 K (Volkamer et al., 2005b); blue and green lines mark the start and end of the optimal wavelength intervals, respectively, with the main absorption bands in the shaded area (bottom).

AMTD
7, 5559–5599, 2014

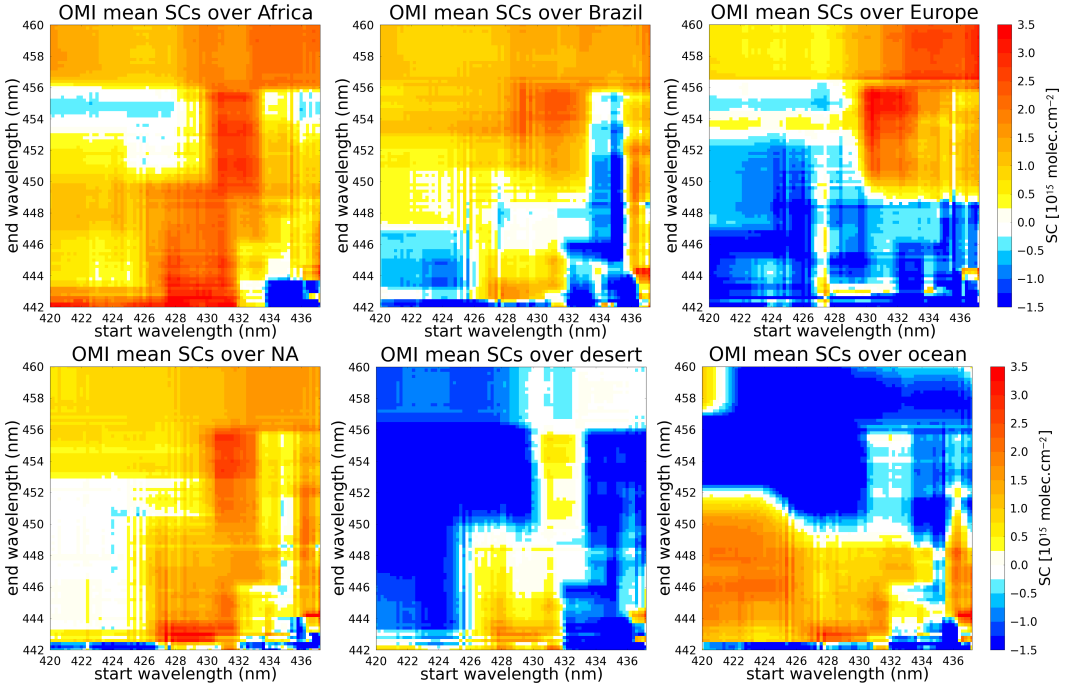

Figure 2. CHOCHO SC means retrieved over selected regions from OMI measurements for wavelength windows with start limits of 420–437 nm and end limits of 442–460 nm, during different days on August 2007 (see Table 1).

AMTD
7, 5559–5599, 2014

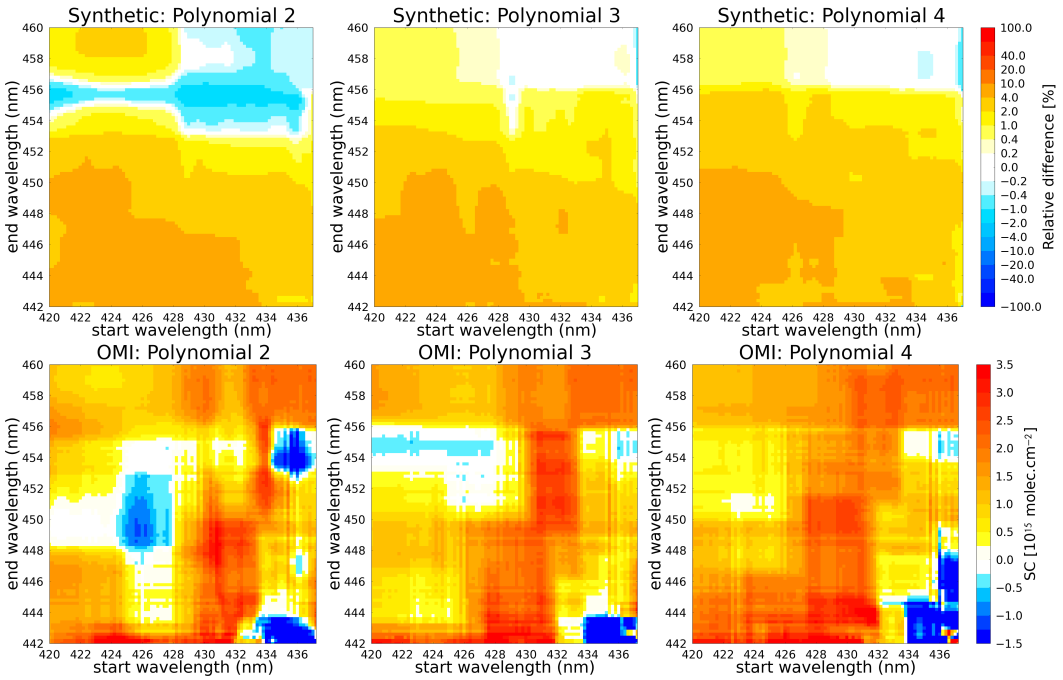

Figure 3. Colour mapping of CHOCHO SC deviation with respect to the a-priori ("true value"), retrieved from a synthetic spectrum for wavelength intervals with start limits of 420–437 nm, end limits 442–460 nm, and polynomial degrees 2, 3, and 4 (top). CHOCHO SC means for 9 August 2007, retrieved over Africa (latitude: $-5.0^{\circ} \pm 3.0^{\circ}$; longitude: $13.5^{\circ} \pm 0.5^{\circ}$) from OMI measurements for different wavelength ranges and polynomial orders (bottom).

AMTD
7, 5559–5599, 2014

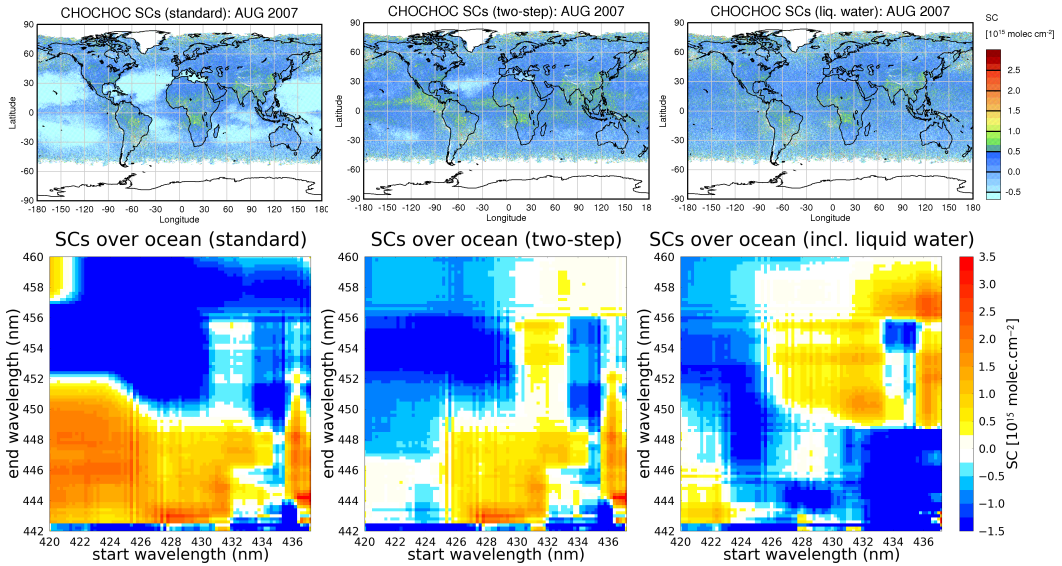

Figure 4. Maps of monthly averaged glyoxal slant columns retrieved from OMI measurements for August 2007 (top). Cloud screening has been applied in all maps (see Sect. 3). CHOCHO SCs obtained using the standard CHOCHO retrieval without liquid water absorption cross-section (left), by using the two-step fit (center), and including the liquid water absorption cross section in the standard CHOCHO retrieval (right). CHOCHO SC means retrieved over Ocean (latitude: 25.0°± 1.0°; longitude: 144.0°± 1.0°) from OMI measurements for the three different retrievals on 1 August 2007 (bottom).

AMTD
7, 5559–5599, 2014

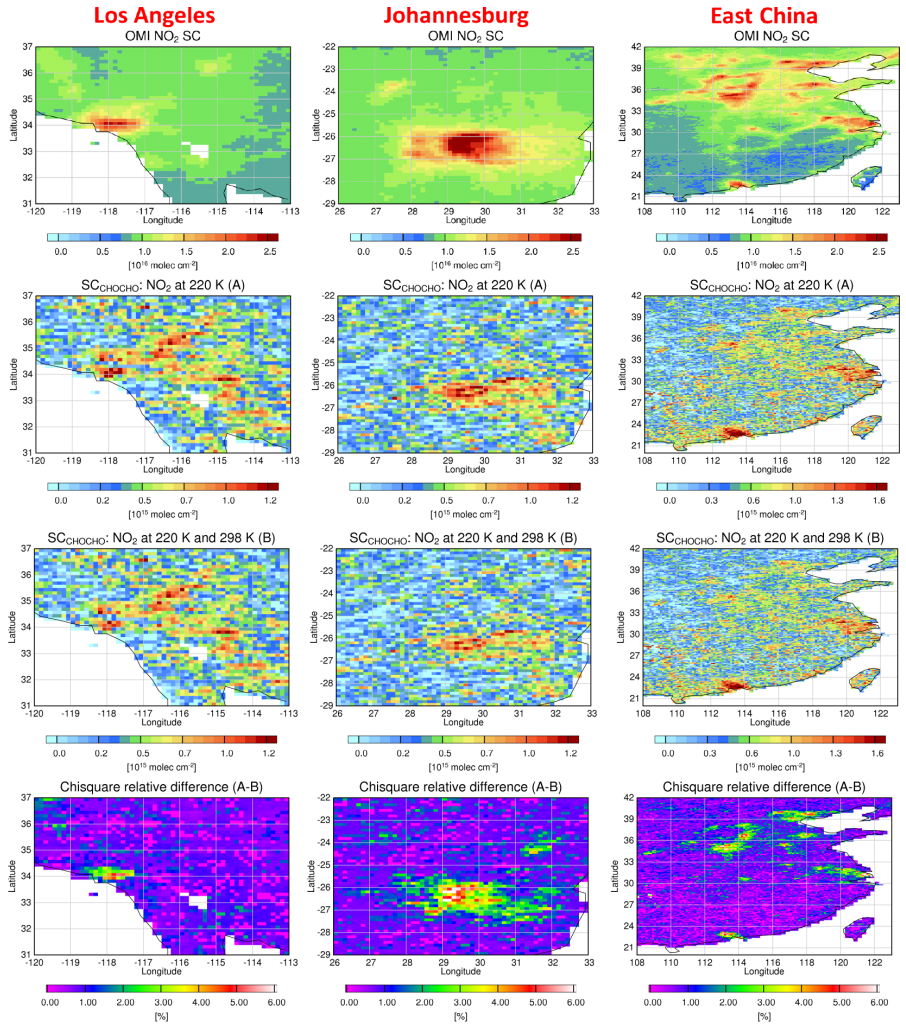

AMTD
7, 5559–5599, 2014

Glyoxal retrieval from OMI

L. M. A. Alvarado et al.

Figure 5. Monthly maps of NO_2 SCs, glyoxal SCs, and chisquare difference between glyoxal retrievals with and without high temperature NO_2 absorption cross-section over Los Angeles, Johannesburg, and East China for September 2007. (A) CHOCHO SCs retrieved with 220 K NO_2 absorption cross-section. (B) An additional NO_2 absorption cross-section at high temperature (298 K) is included in the glyoxal retrieval.

AMTD
7, 5559–5599, 2014

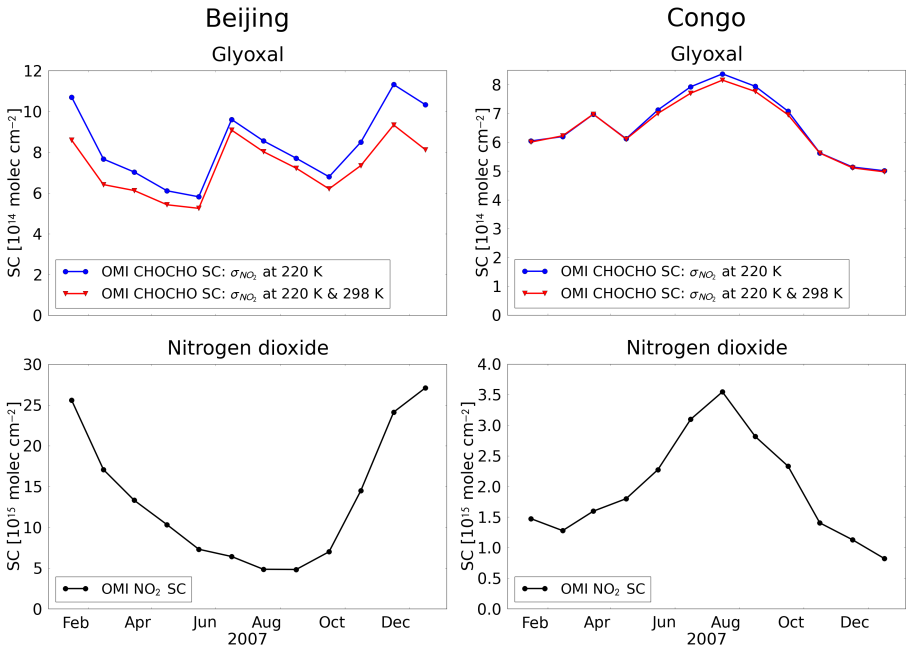

Figure 6. Seasonal variation of glyoxal SCs including and excluding the high-temperature NO_2 absorption cross-section (top), NO_2 SCs (bottom) over Beijing (latitude: $37.5^\circ \pm 2.5^\circ$; longitude: $115.5^\circ \pm 1.5^\circ$) and Congo (latitude: $-4.0^\circ \pm 2.0^\circ$; longitude: $18.0^\circ \pm 2.0^\circ$) for 2007.

AMTD
7, 5559–5599, 2014

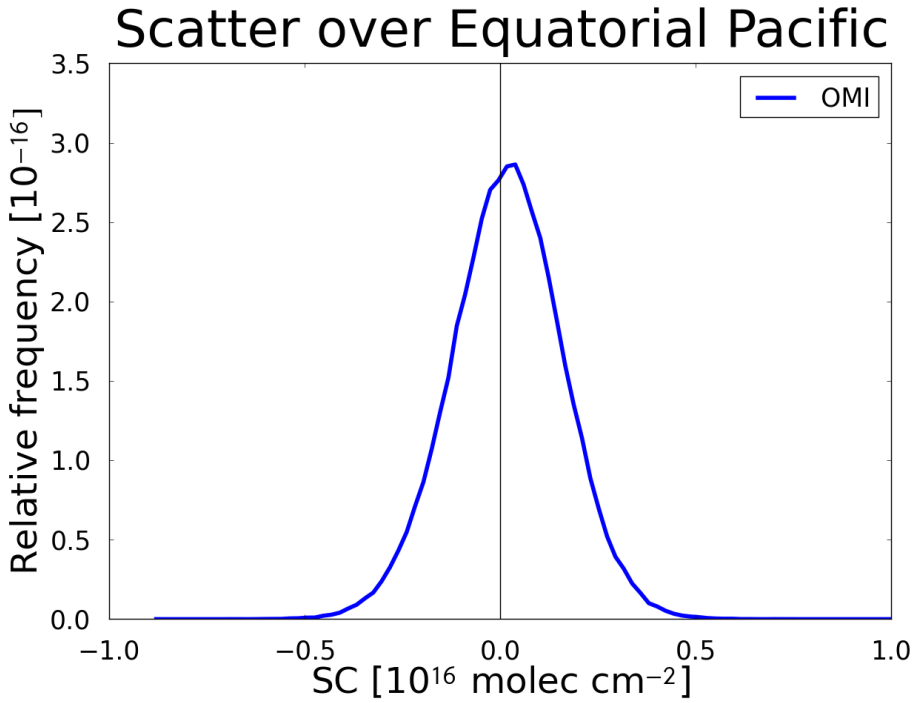

Figure 7. Distribution of CHOCHO SCs over a clean ocean region at the equatorial (5° S–5° N, 160–200° E) for August 2007.

AMTD
7, 5559–5599, 2014

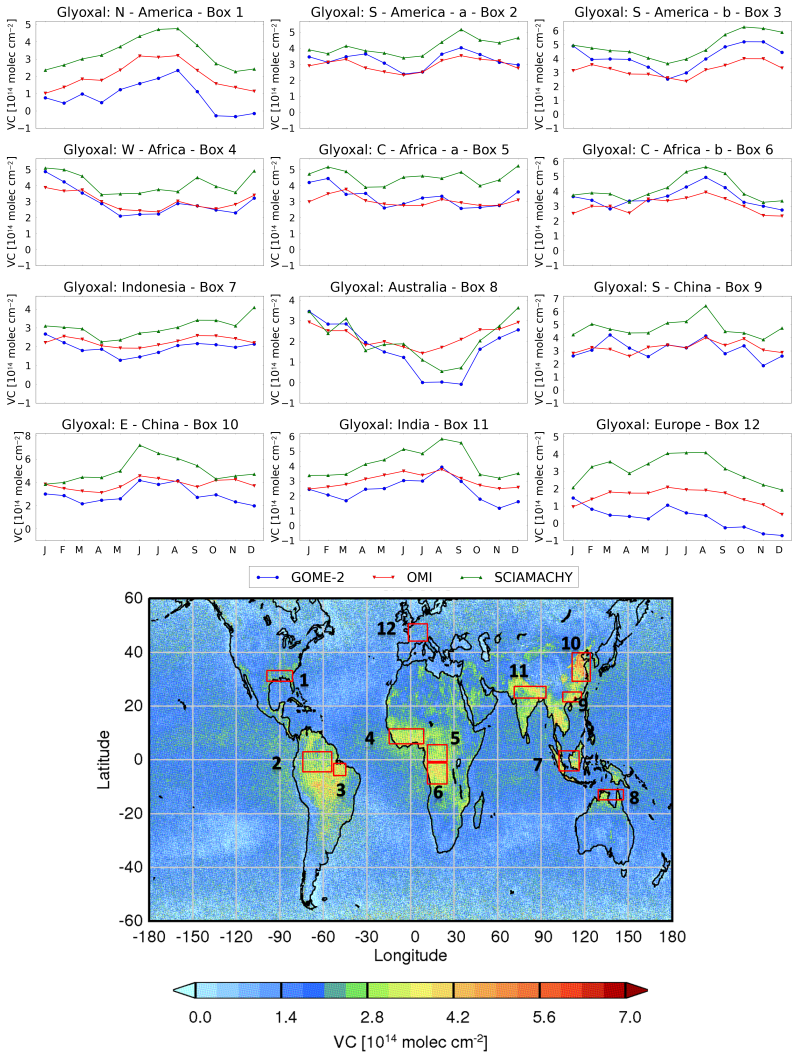

AMTD
7, 5559–5599, 2014

Glyoxal retrieval from OMI

L. M. A. Alvarado et al.

Figure 8. Comparison of monthly averaged CHOCHO VCs from OMI (red line), GOME-2 (blue line) and SCIAMACHY (green line) data for 12 selected regions (boxes 1–12) for 2007 (top). Annual global CHOCHO map with 12 selected regions for different environments (bottom).

AMTD
7, 5559–5599, 2014

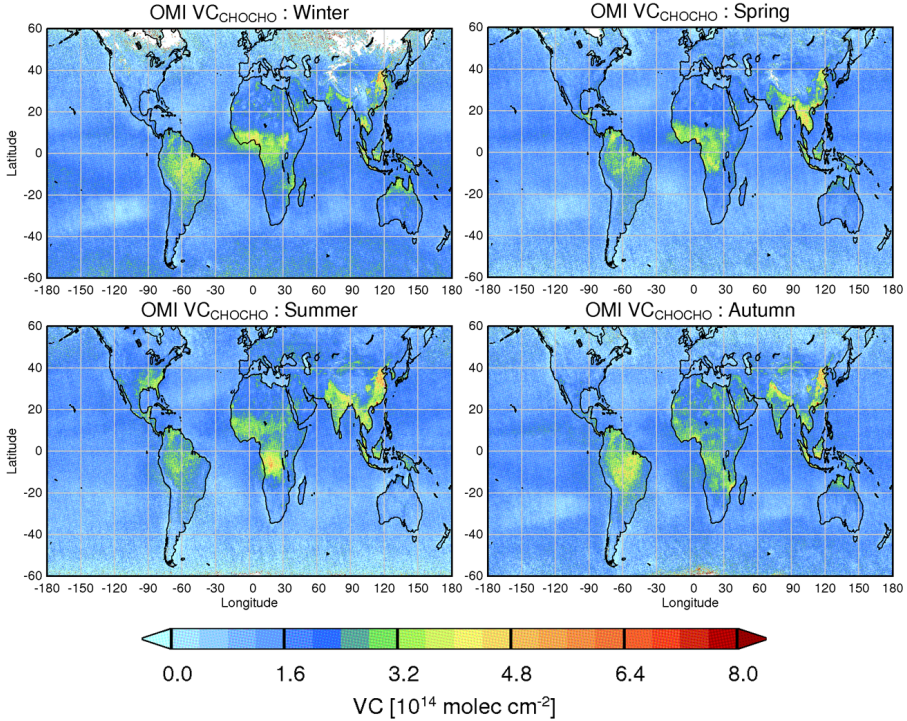

Figure 9. Seasonal means of CHOCHO VCs for winter (DJF), spring (MAM), summer (JJA), autumn (SON) for 2005–2013.

AMTD
7, 5559–5599, 2014

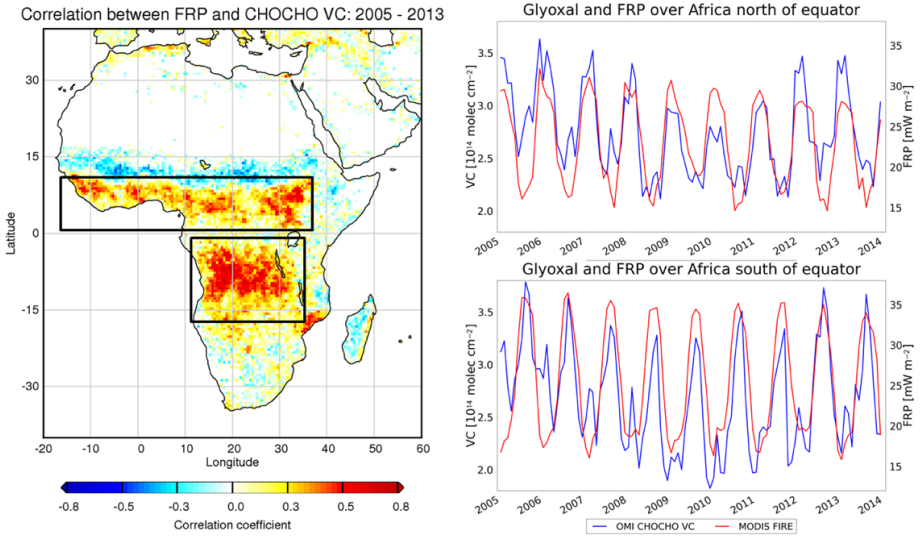

Figure 10. Pearson correlation map (left) and seasonal variation (right) of FRP and CHOCHO VC over Africa from 2005 to 2013.

AMTD
7, 5559–5599, 2014

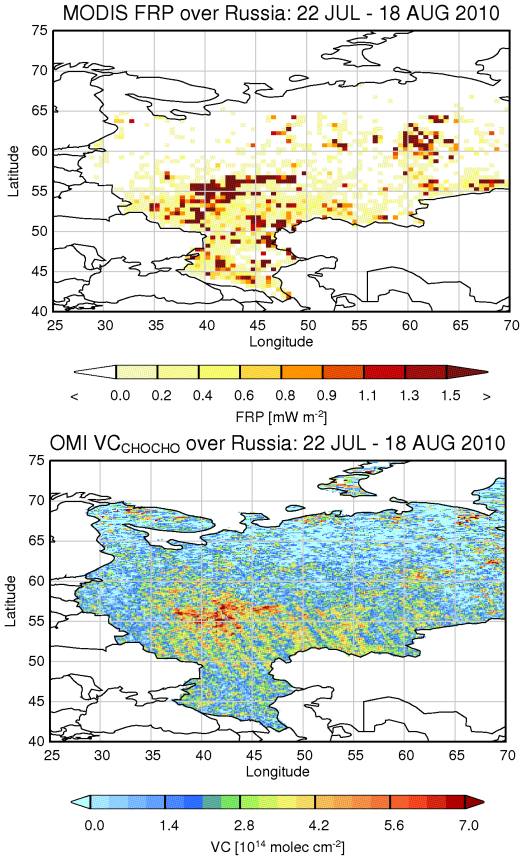

Figure 11. Maps of fire radiative power (top) and glyoxal VCs (bottom) over Russia from 22 July to 18 August 2010.

AMTD
7, 5559–5599, 2014